An integrated pan-tropical biomass map using multiple reference datasets

An integrated pan-tropical biomass map using multiple reference datasets

(PAN-TROPICAL FUSED BIOMASS MAP)

Avitabile V. [1], Herold M. [1], Heuvelink G.B.M. [1], Lewis S.L. [2,3], Phillips O.L. [2], Asner G.P. [4], Armston J. [5,6], Asthon P.[7,8], Banin L.F.[9], Bayol N. [10], Berry N.[11], Boeckx P.[12], de Jong B. [13], DeVries B. [1], Girardin C. [14], Kearsley E. [12,15], Lindsell J.A. [16], Lopez-Gonzalez G. [2], Lucas R. [17], Malhi Y. [14], Morel A. [14], Mitchard E. [11], Nagy L. [18], Qie L.[2], Quinones M. [19], Ryan C.M. [11], Slik F. [20], Sunderland, T. [21], Vaglio Laurin G. [22], Valentini R. [23], Verbeeck H. [12], Wijaya A. [21], Willcock S. [24]

1. Wageningen University, the Netherlands; 2. University of Leeds, UK; 3. University College London, UK; 4. Carnegie Institution for Science, USA; 5. The University of Queensland, Australia; 6. Information Technology and Innovation, Australia; 7. Harvard University, UK; 8. Royal Botanic Gardens, UK; 9. Centre for Ecology and Hydrology, UK; 10. Foret Ressources Management, France; 11. University of Edinburgh, UK; 12. Ghent University, Belgium; 13. Ecosur, Mexico; 14. University of Oxford, UK; 15. Royal Museum for Central Africa, Belgium; 16. The RSPB Centre for Conservation Science, UK; 17. The University of New South Wales, Australia; 18. Universidade Estadual de Campinas, Brazil; 19. SarVision, the Netherlands; 20. Universiti Brunei Darussalam, Brunei; 21. Center for International Forestry Research, Indonesia; 22. Centro Euro-Mediterraneo sui Cambiamenti Climatici, Italy; 23. Tuscia University, Italy; 24. University of Southampton, UK

Correspondence: Valerio Avitabile, tel. +31 317482092, email: valerio.avitabile@wur.nl

Keywords: aboveground biomass, carbon cycle, forest plots, tropical forest, forest inventory, REDD+, satellite mapping, remote sensing

Type of paper: Primary Research Article

Abstract

We combined two existing datasets of vegetation aboveground biomass (AGB) (Saatchi et al., 2011; Baccini et al., 2012) into a pan-tropical AGB map at 1-km resolution using an independent reference dataset of field observations and locally-calibrated high-resolution biomass maps, harmonized and upscaled to 14,477 1-km AGB estimates. Our data fusion approach uses bias removal and weighted linear averaging that incorporates and spatializes the biomass patterns indicated by the reference data. The method was applied independently in areas (strata) with homogeneous error patterns of the input (Saatchi and Baccini) maps, which were estimated from the reference data and additional covariates. Based on the fused map, we estimated AGB stock for the tropics (23.4 N – 23.4 S) of 375 Pg dry mass, 9% - 18% lower than the Saatchi and Baccini estimates. The fused map also showed differing spatial patterns of AGB over large areas, with higher AGB density in the dense forest areas in the Congo basin, Eastern Amazon and South-East Asia, and lower values in Central America and in most dry vegetation areas of Africa than either of the input maps. The validation exercise, based on 2,118 estimates from the reference dataset not used in the fusion process, showed that the fused map had a RMSE 15 – 21% lower than that of the input maps and, most importantly, nearly unbiased estimates (mean bias 5 Mg dry mass ha^{-1} vs. 21 and 28 Mg ha^{-1} for the input maps). The fusion method can be applied at any scale including the policy-relevant national level, where it can provide improved biomass estimates by integrating existing regional biomass maps as input maps and additional, country-specific reference datasets.

Introduction

Recently, considerable efforts have been made to better quantify the amounts and spatial distribution of aboveground biomass (AGB), a key parameter for estimating carbon emissions and removals due to land-use change, and related impacts on climate (Saatchi et al., 2011; Baccini et al., 2012; Harris et al., 2012; Houghton et al., 2012; Mitchard et al., 2014; Achard et al., 2014). Particular attention has been given to the tropical regions, where uncertainties are higher (Pan et al., 2011; Ziegler et al., 2012; Grace et al., 2014). In addition to ground observations acquired by research networks or for forest inventory purposes, several AGB maps have been recently produced at different scales, using a variety of empirical modelling approaches based on remote sensing data calibrated by field observations (e.g., Goetz et al., 2011; Birdsey et al., 2013). AGB maps at moderate resolution have been produced for the entire tropical belt by integrating various satellite observations (Saatchi et al., 2011; Baccini et al., 2012), while higher resolution datasets have been produced at local or national level using medium-high resolution satellite data (e.g., Avitabile et al., 2012; Cartus et al., 2014), sometimes in combination with airborne Light Detection and Ranging (LiDAR) data (Asner et al., 2012a, 2012b, 2013, 2014a). The various datasets often have different purposes: research plots provide a detailed and accurate estimation of AGB (and other ecological parameters or processes) at the local level, forest inventory networks use a sampling approach to obtain statistics of biomass stocks (or growing stock volume) per forest type at the sub-national or national level, while high-resolution biomass maps can provide detailed and spatially explicit estimates of AGB density to assist natural resource management, and large scale coarse-resolution datasets depict AGB distribution for global-scale carbon accounting and modelling.

In the context of the United Nations mechanism for Reducing Emissions from Deforestation and forest Degradation (REDD+), emission estimates obtained from spatially explicit biomass datasets may be favoured over those based on mean values derived from plot networks. This preference stems from the fact that plot networks are not designed to represent land cover change events, which usually do not occur randomly and may affect forests with biomass density systematically different from the mean value (Baccini and Asner, 2013). With very few tropical countries having national AGB maps or reliable statistics on forest carbon stocks, regional maps may provide advantages compared to the use of default mean values (e.g., IPCC (2006) Tier 1 values) to assess emissions from deforestation, as long as their accuracy is reasonable and their estimates are not affected by systematic errors (Avitabile et al., 2011). These conditions are difficult to assess, however, since rigorous validation of regional AGB maps remains problematic, given their large area coverage and large mapping unit (Mitchard et al., 2013), while ground observations are only available for a limited number of small sample areas.

The comparison of two recent pan-tropical AGB maps (Saatchi et al., 2011; Baccini et al., 2012) revealed substantial differences between the two products (Mitchard et al., 2013). Further comparison with ground observations and high-resolution maps also highlighted notable differences in AGB patterns at regional scales (Baccini and Asner, 2013; Hills et al., 2013; Mitchard et al., 2014). Such comparisons have stimulated a debate over the use and capabilities of different types of biomass products (Saatchi et al., 2014; Langner et al., 2014) and have highlighted both the importance and sometimes the lack of integration of different datasets. On one hand, the two pan-tropical maps are consistent in terms of methodology because both use the same primary data source (GLAS LiDAR) alongside a similar modelling approach to upscale the LiDAR data to larger scales. Moreover, they have the advantage of

98 being calibrated using hundreds of thousands of AGB estimates derived from height metrics
99 computed by a spaceborne LiDAR sensor distributed over the tropics. However, such maps
100 are based on remotely sensed variables that do not directly measure AGB, but are sensitive to
101 canopy cover and canopy height parameters that do not fully capture the AGB variability of
102 complex tropical forests. Furthermore, both products assume global or continental allometric
103 relationships in which AGB varies only with stand height, and further errors are introduced by
104 upscaling the calibration data to the coarser satellite data. On the other hand, ground plots use
105 allometric equations to estimate AGB at individual tree level using directly measurable
106 parameters such as diameter, height and species identity (hence wood density). However, they
107 have limited coverage, are not error-free, and compiling various datasets over large areas is
108 made more complex due to differing sampling strategies (e.g., stratification of landscapes,
109 plot size, minimum diameter of trees measured). Considering the rapid increase of biomass
110 observations at different scales and the different capabilities and limitations of the various
111 datasets, it is becoming more and more important to identify strategies that are capable of
112 making best use of existing information and optimally integrate various data sources for
113 improved large area AGB assessment (e.g., see Willcock et al., 2012).
114
115 In the present study, we compiled existing ground observations and locally-calibrated high-
116 resolution biomass maps to obtain a high-quality AGB reference dataset for the tropical
117 region (Objective 1). This reference dataset was used to assess two existing pan-tropical AGB
118 maps (Objective 2) and to combine them in a fused map that optimally integrates the two
119 maps, based on the method presented by Ge et al. (2014) (Objective 3). Lastly, the fused map
120 was assessed and compared to known AGB stocks and patterns across the tropics (Objective
121 4).
122

Overall, the approach consisted of pre-processing, screening and harmonizing the pan-tropical AGB maps (called 'input maps'), the high-resolution AGB maps (called 'reference maps') and the field plots (called 'reference plots'; 'reference dataset' refers to the maps and plots combined) to a common spatial resolution and geospatial reference system (Figure 1). The input maps were combined using bias removal and weighted linear averaging ('fusion'). The fusion model was applied independently to areas associated with different error patterns of the input maps (called 'error strata'), which were estimated from the reference data and additional covariates (called 'covariate maps'). The reference dataset included only a subset of the reference maps (i.e., the cells with highest confidence) and if a stratum was lacking reference data ('reference data gaps'), additional data were extracted from the reference maps ('consolidation'). The fused map was validated using independent data and its uncertainty quantified using model parameters. In this study, the terms AGB refers to aboveground live woody biomass and is reported in units of Mg dry mass ha^{-1}. The fused map and the corresponding reference dataset can be freely downloaded from www.wageningenur.nl/grsbiomass.

Materials and methods

Input maps

The input maps used for this study were the two pan-tropical datasets published by Saatchi et al. (2011) and Baccini et al. (2012), hereafter referred to as the "Saatchi" and "Baccini" maps individually, or as "input" maps collectively. The Baccini map was provided in MODIS sinusoidal projection with a spatial resolution of 463 m while the Saatchi map was in a geographic projection (WGS-84) at 0.00833 degrees (approximately 1 km) pixel size. The two datasets were harmonized by first projecting the Baccini map to the coordinate system of the Saatchi map using the Geospatial Data Abstraction Library (www.gdal.org) and then aggregating it to match the spatial resolution and grid of the Saatchi map. Spatial aggregation was performed by computing the mean value of the pixels whose centre was located within each 1-km cell of the Saatchi map. Resampling was then undertaken using the nearest neighbor method.

Reference dataset

The reference dataset comprised individual tree-based field data and high-resolution AGB maps independent from the input maps. The field data included AGB estimates derived from field measurement of tree parameters and allometric equations. The AGB maps included high-resolution (≤ 100 m) datasets derived from satellite data using empirical models calibrated and validated using local ground observations and, in some cases, airborne LiDAR measurements. Given the variability of procedures used to acquire and produce the various datasets, they were first screened according to a set of quality criteria to select only the most reliable AGB estimates, and then pre-processed to be harmonized with the pan-tropical AGB maps in terms of spatial resolution and observed variables. Field and map datasets providing aboveground carbon density were converted to AGB units using the same coefficients used

for their original conversion from biomass to carbon. The sources and characteristics of the reference data are listed in the Supplementary Information (Tables S8 - S11).

Data screening and pre-processing

Reference field data

The reference field data were measurements from forest inventory plots for which accurate geolocation and biomass estimates were available. Pre-processing of the data consisted of a 2-step screening and a harmonization procedure. A preliminary screening selected only the ground data that satisfied the following criteria: (1) they estimated AGB for all living trees with diameter at breast height ≥ 5-10 cm; (2) they were acquired on or after the year 2000; (3) they were not used to calibrate the LiDAR-AGB relationships of the input maps; and (4) their plot coordinates were measured using a GPS. Since the taxonomic identities of trees strongly indicate wood density, and hence stand-level biomass (e.g., Baker et al., 2004; Mitchard et al. 2014), plots were only selected if tree AGB was estimated using at least tree diameter and wood density as input parameters. Datasets were excluded if they did not conform to these requirements or did not provide clear information on the biomass pool measured, the tree parameters measured in the field, the allometric model applied, the year of measurement or the plot geolocation and extent. Next, the plot data were projected to the geographic reference system WGS-84 and harmonized with the input maps by averaging the AGB values located within the same 1-km pixel if there was more than one plot per pixel, or by directly attributing the plot AGB to the respective pixel if there was only one plot per pixel. Field plots not fully located within one pixel were attributed to the map cell where the majority of the plot area (i.e., the plot centroid) was located.

197 Lastly, the representativeness of the plot over the 1-km pixels was considered, and the ground
198 data were further screened to discard plots not representative of the map cells in terms of
199 AGB density. More specifically, since the two input maps in their native reference systems
200 are not aligned and therefore their pixels do not correspond to the same geographic area, the
201 plot representativeness was assessed on the area of both pixels (identified before the map
202 resampling). The representativeness was evaluated on the basis of the homogeneity of the tree
203 cover and crown size within the pixel, determined through visual interpretation of high-
204 resolution images provided on the Google Earth platform. If the tree cover and tree crowns
205 were not homogeneous over at least 90% of the pixel area, the plots located within the pixel
206 were discarded (Fig. S1). In addition, if subsequent Google Earth images indicated that forest
207 change processes (e.g., deforestation or regrowth) occurred in the period between the field
208 measurement and the reference years of the input maps, the corresponding plots were
209 discarded.
210
211 *Reference biomass maps*
212 The reference biomass maps consisted of high-resolution local or national AGB maps
213 published in the scientific literature. Maps providing AGB estimates grouped in classes (e.g.,
214 Willcock et al., 2012) were not used since the class values represent the mean AGB over large
215 areas, usually spanning multiple strata used in the present study (see 'Stratification approach').
216 The reference AGB maps were first pre-processed to match the input maps through re-
217 projection, aggregation and resampling using the same procedures described for the pre-
218 processing of the Baccini map. Then, only the cells with largest confidence (i.e., lowest
219 uncertainty) were selected from the maps. Since uncertainty maps were usually not available,
220 and considering that the reference maps were based on empirical models, the map cells with
221 greatest confidence were assumed to be those in correspondence of the training data (field

222 plots and/or LiDAR data). When the locations of the training data were not available, random
223 pixels were extracted from the maps. For maps based only on radar or optical data, whose
224 signals saturate above a certain AGB density value, only pixels below such a threshold were
225 considered. In order to compile a reference database that was representative of the area of
226 interest and well-balanced among the various input datasets (as defined in 'Consolidation of
227 the reference dataset'), the amount of reference data extracted from the AGB maps was
228 proportional to their area and not greater than the amount of samples provided by the field
229 datasets representing a similar area. In the case where maps with extensive training areas
230 provided a disproportionate number of reference pixels, a further screening selected only the
231 areas underpinned by the largest amount of training data.
232
233 **Consolidation of the reference dataset**
234 Considering that the modelling approach used in this study is applied independently by
235 stratum (which represent areas with homogeneous error structure in both input maps; see
236 'Stratification approach') and is sensitive to the characteristics of the reference data (see
237 'Modelling approach'), each stratum requires that calibration data are relatively well-balanced
238 between the various reference datasets. Specifically, if a stratum contains few calibration data,
239 the model becomes more sensitive to outliers, while if a reference dataset is much larger than
240 the others, the model is more strongly determined by the dominant dataset. For these reasons,
241 for the strata where the reference dataset was under-represented or un-balanced, it was
242 consolidated by additional reference data taken from the reference AGB maps, if available.
243 The reference data were considered insufficient if a stratum had less than half of the average
244 reference data per stratum, and were considered un-balanced if a single dataset provided more
245 than 75% of the reference data of the whole stratum and it was not representative of more than
246 75% of its area. In such cases, additional reference data were randomly extracted from the

247 reference AGB maps that did not provide more than 75% of the reference data. The amount of
248 data to be extracted from each map was computed in a way to obtain a reference dataset with
249 an average number of reference data per stratum and not dominated by a single dataset. If
250 necessary, additional training data representing areas with no AGB (e.g., bare soil) were
251 included, using visual analysis of Google Earth images to identify locations without
252 vegetation.
253
254 **Selected reference data**
255 The AGB reference dataset compiled for this study consisted of 14,477 1-km reference pixels,
256 distributed as follows: 953 in Africa, 449 in South America, 7,675 in Central America, 400 in
257 Asia and 5,000 in Australia (Fig. 2, Table 1). The reference data were relatively uniformly
258 distributed among the strata (Table S6) but their amount varied considerably by continent.
259 The average amount of reference data per stratum ranged from 50 (Asia) to 958 (Central
260 America) 1-km reference pixels and their variability (computed as standard deviation relative
261 to the mean) ranged from 25% (South America) to 52% (Central America). The uneven
262 distribution of reference data across the continents is mostly caused by the availability of
263 ground observations: as indicated above, in order to have a balanced reference dataset for
264 each stratum the reference data extracted from AGB maps were limited to the (smaller)
265 amount of direct field observations. When AGB maps were the only source of data, this
266 constraint was not occurring and larger datasets could be derived from the maps (i.e., Central
267 America, Australia).
268
269 The reference data were selected from 18 ground datasets and from 9 high-resolution AGB
270 maps calibrated by field observations and, in 4 cases, airborne LiDAR data (Table 1). The
271 field plots used for the calibration of the maps are not included in this section because they

were only used to select the reference pixels from the maps. The visual screening of the field plots removed 35% of the input data (from 6,627 to 4,283) and their aggregation to 1-km resolution further removed 70% of the reference units derived from field plots (from 4,283 to 1,274), while 10,741 reference pixels were extracted from the high-resolution AGB maps. The criteria used to select the reference pixels for each map are reported in Table S2. The consolidation procedure was necessary only for Central America where it added 2,415 reference data, while 47 pixels representing areas with no AGB were identified in Asia (Table S1). In general, ground observations were mostly discarded in areas characterized by fragmented or heterogeneous vegetation cover and high biomass spatial variability. In such contexts, reference data were often acquired from the AGB maps.

Stratification approach

Preliminary comparison of the reference data with the input maps showed that the error variances and biases of the input maps were not spatially homogeneous but varied considerably in different regions. Since the fusion model used in this study (see 'Modelling approach') is based on bias removal and weighted combination of the input maps, the more homogeneous the error characteristics in the input maps are, the better they can be reduced by the model. For this reason, the stratification approach aimed at identifying areas with homogeneous error structure (hereafter named 'error strata') in both input maps. A first stratification was undertaken based on geographic location (namely Central America, South America, Africa, Asia and Australia) to reflect the regional allometric relationships between AGB and tree diameter and height (Feldpausch et al., 2011, 2012). Then, the error strata were identified for each continent using a two-step process. First, the error maps of the Saatchi and Baccini maps were predicted separately. Since the AGB estimates of the input maps were mostly based on optical and LiDAR data that are sensitive to tree cover and tree height, it was

297 assumed that their uncertainties were related to the spatial variation of these parameters. In
298 addition, the errors of the input maps were found to be linearly correlated with the respective
299 AGB estimates. For these reasons, the AGB maps themselves, as well as global datasets of
300 land cover (ESA, 2014a), tree cover (Di Miceli et al., 2014) and tree height (Simard et al.,
301 2011), were used to predict the map errors using a Random Forest model (Breiman, 2001)
302 calibrated on the basis of the reference dataset. Second, the error maps of the Saatchi and
303 Baccini datasets were clustered using the K-Means approach. The use of eight clusters (hence,
304 eight error strata) was considered a sensible trade-off between homogeneity of the errors of
305 the input maps and number of reference observations available per stratum, with a larger
306 number of clusters providing only a marginal increase in homogeneity but leading to a small
307 number of reference data in some strata (Fig. S2). In areas where the predictors presented no
308 data (i.e., outside the coverage of the Baccini map) or for classes of the categorical predictor
309 without reference data (i.e., land cover), the error strata (instead of the error maps) were
310 predicted using an additional Random Forest model based on predictors without missing
311 values (i.e., Saatchi map, tree cover and tree height) and 10,000 training data randomly
312 extracted from the stratification map.
313
314 This method produced a stratification map that identified eight strata for each continent with
315 homogeneous error patterns in the input maps (Fig. S3). The root mean square error (RMSE)
316 computed on the Out-Of-Bag data (i.e., data not used for training) of the Random Forest
317 models that predicted the errors of the input maps ranged between 22.8 ± 0.3 Mg ha^{-1} (Central
318 America) to 83.7 ± 2.5 Mg ha^{-1} (Africa), with the two models (one for each input map)
319 achieving similar accuracies in each continent (Table S4, Fig. S4). In most cases the main
320 predictors of the errors of the input maps were the biomass values of the maps themselves,
321 followed by tree cover and tree height, while land cover was always the least important

322 predictor (Table S5). Further details on the processing of the input data are provided in the
323 Supplementary Information.
324
325 The use of a stratification based on the errors of the input maps was compared with
326 stratifications based on land cover (used by Ge et al., 2014), tree cover and tree height. A
327 separate stratification map was obtained for each of these alternative variables by aggregation
328 into eight strata (to maintain comparability with the number of clusters used in the error
329 strata), and each stratification map was used to develop a specific fused map. The
330 performance of alternative stratification approaches was assessed by validating the respective
331 fused maps (see Supplementary Information – Alternative stratification approaches). The
332 results demonstrated that the stratification based on error modelling and clustering (i.e., the
333 error strata) produced a fused map with higher accuracy than that of the maps based on other
334 stratification approaches, and therefore was used in this study (Fig. S5).
335
336 ***Modelling approach***
337 **The fusion model**
338 The integration of the two input maps was performed with a fusion model based on the
339 concept presented by Ge et al. (2014) and further developed for this study. The fusion model
340 consists of bias removal and weighted linear averaging of the input maps to produce an output
341 with greater accuracy than each of the input maps. The reference AGB dataset described
342 above was used to calibrate the model and to assess the accuracy of the input and fused maps.
343 A specific model was developed for each stratum.
344
345 Following Ge et al. (2014), the p input maps for locations $s \in D$, where D is the geographical
346 domain of interest common to the input maps, were combined using a weighted linear average:

$$(1)\quad f(s) = \sum_{i=1}^{p} w_i(s) \cdot (z_i(s) - v_i(s))$$

where f is the fused map, the $w_i(s)$ are weights, z_i the estimate of the i-th input map and $v_i(s)$ is the bias estimate. The bias term was computed as the average difference between the input map and the reference data for each stratum. The weights were obtained from a statistical model that assumes the map estimates z_i to be the sum of the true biomass b_i with a bias term v_i and a random noise term ε_i with zero mean for each location $s \in D$. We further assumed that the ε_i of the input maps are jointly normally distributed with variance-covariance matrix $\boldsymbol{C}(s)$. Differently from Ge et al. (2014), $\boldsymbol{C}(s)$ was estimated using a robust covariance estimator as implemented by the 'robust' package in R (Wang et al., 2014), which uses the Stahel-Donoho estimator for strata with fewer than 5,000 observations and the Fast Minimum Covariance Determinant estimator for larger strata. Under these assumptions, the variance of the estimation error of the fused map $f(s)$ is minimized by calculating the weights $w(s)$ as outlined by Searle (1971, p. 89):

$$(2)\quad w(s)^T = \left(\mathbf{1}^T \mathbf{C}(s)^{-1} \mathbf{1}\right)^{-1} \mathbf{1}^T \mathbf{C}(s)^{-1}$$

where $\mathbf{1}=[1, ..., 1]^T$ is the transpose of the p-dimensional unit vector. The weights computed for each stratum sum to 1, while their values are approximately inversely proportional to the error variance of the corresponding input map. Larger weights are assigned to input maps with lower error variances, although the covariance between map errors influences the weights as well. Overall, the fused map is expected to provide more accurate estimates after bias removal and weighted averaging of the input maps. The fusion model assured that the variance of the error in the fused map was smaller than that of the input maps (Bates and Granger, 1969), especially if the errors associated with these maps were not strongly positively correlated and their error variances were close to the smallest error variance. The fusion model can be applied to any number of input maps. Where there is only one input map, the model estimates and removes its bias and the weights are set equal to 1.

372

373 **The model parameters**

374 The fusion model computed a set of bias and weight parameters for each stratum and
375 continent on the basis of their respective reference data, and used these for the linear weighted
376 combination of the input maps (Table S6). Since the stratification approach grouped together
377 data with similar error patterns, the biases varied considerably among the strata and could
378 reach values up to ±200 Mg ha^{-1}. However, considering the area of the strata, the biases of
379 both input maps were smaller than ±45 Mg ha^{-1} for at least 50% of the area of all continents
380 and smaller than ±100 Mg ha^{-1} for 81% - 98% of the area of all continents.

381

382 ***Post-processing***

383 **Predictions outside the coverage of the Baccini map**

384 The Baccini map covers the tropical belt between 23.4 degree north latitude and 23.4 degree
385 south latitude while the Saatchi map presents a larger latitudinal coverage (Fig. 2). The fusion
386 model was first applied to the area common to both input maps (Baccini extent) and then
387 extended to the area where only the Saatchi map is available. In the latter area, the model
388 focused only on removing the bias of the Saatchi map using the values estimated for the
389 Baccini extent. The model predictions for the Saatchi extent were mosaicked to those for the
390 Baccini extent using a smoothing function (inverse distance weight) on an overlapping area of
391 1 degree within the Baccini extent between the two maps. Water bodies were masked over the
392 whole study area using the ESA CCI Water Bodies map (ESA, 2014b). The resulting fused
393 map was projected to an equal area reference system (MODIS Sinusoidal) before computing
394 the total AGB stocks for each continent, which were obtained by summing the products of the
395 AGB density of each pixel with their area.

396

Assessing AGB in intact and non-intact forest

The AGB estimates of the fused and input maps in forest areas were further investigated regarding their distribution in ecozones and between intact and non-intact landscapes. Forest areas were defined as areas dominated by tree cover according to the GLC2000 map (Bartholomé and Belward, 2005). Ecozones were defined according to the Global Ecological Zone (GEZ) map for the year 2000 (FAO, 2000). The intact landscapes were defined according to the Intact Forest Landscape (IFL) map for the year 2000 (Potapov et al., 2008). On the basis of these datasets, the mean forest AGB density of the fused and input maps were computed for intact and non-intact landscapes for each continent and major ecozone. To allow direct comparison of the results among the maps, the analysis was performed only for the area common to all maps (Baccini extent). In addition, to reduce the impact of spatial inaccuracies in the maps, only ecozones with IFL intact forest areas larger than 1,000 km^2 were considered. The mean AGB density of intact and non-intact forests per continent was computed as the area-weighted mean of the contributing ecozones.

Validation and uncertainty

Validation of the fused and input maps was performed by randomly splitting the reference data into a calibration set (70% of the data) and a validation set (remaining 30%). The 'final' fused map presented in Fig. 3 used 100% of the reference data while for validation purposes a 'test' fused map was produced using only the calibration data. The estimates of the 'test' fused map, as well as those of the input maps, were compared with the validation data. Note that validation of the 'test' fused map only yields an approximate (i.e., conservative) estimate of the accuracy of the 'final' fused map. In other words, the 'final' fused map is likely more accurate than the 'test' fused map because it uses a larger calibration data set. To maintain full independence, validation data were not used for any step related to the development of the

422 'test' fused map, including production of the stratification map. To account for any potential
423 impacts of the random selection of validation data, the procedure was repeated 100 times,
424 computing a new random selection of the calibration and validation datasets with each
425 iteration. This procedure allowed computing the mean RMSE and assessing its standard
426 deviation for the fused and input maps.
427
428 The uncertainty of the fused map was computed with respect to model uncertainty, not
429 including the error sources in the input data (see 'Discussion'). The model uncertainty
430 consisted of the expected variance of the error of the fused map (which is assumed to be bias-
431 free) and was derived for each stratum from $\boldsymbol{C}(s)$. The uncertainty was thus estimated per
432 strata and not at the pixel level. The error variance was converted to an uncertainty map by
433 reclassifying the stratification map, where the stratum value was converted to the respective
434 error variance computed for each stratum and continent.
435
436
437
438
439
440
441
442
443
444
445
446

Results

Biomass map

The fusion model produced an AGB map at 1-km resolution for the tropical region, with an extent equal to that of the Saatchi map (Fig. 3). In terms of stocks, the AGB estimates within the fused map were lower than both input maps at continental level. The total stock of the fused map for the tropical belt covered by the Baccini map (23.4 N – 23.4 S, see Fig. 2) was 375 Pg dry mass, 9% and 18% lower than the Saatchi (413 Pg) and Baccini (457 Pg) estimates, respectively. Considering the larger extent of the Saatchi map, the fused map estimate was 462 Pg, 15% lower than the estimate of the Saatchi map (545 Pg) (Table S7).

Moreover, the fused map presented spatial patterns that differed substantially from both input maps (Fig. 4): the AGB estimates were higher than the Saatchi and Baccini maps in the dense forest areas in the Congo basin, in West Africa, in the north-eastern part of the Amazon basin (Guyana shield) and in South-East Asia, and lower in Central America and in most dry vegetation areas of Africa. In the central part of the Amazon basin the fused map showed lower estimates than the Baccini map and higher estimates than the Saatchi map, while in the southern part of the Amazon basin these differences were inversed. Similar trends emerged when comparing the maps separately for intact and non-intact forest ecozones (Supporting Information). In addition, the average difference between intact and non-intact forests was larger than that derived from the input maps in Africa and Asia, similar or slightly larger in South America, and smaller in Central America (Fig. S6).

According to the fused map, the highest AGB density (> 400 Mg ha^{-1}) is found in the Guyana shield, in the central and western part of the Congo basin and in the intact forest areas of Borneo and Papua New Guinea. The analysis of the distribution of forest AGB in intact and

non-intact ecozones showed that the mean AGB density was greatest in intact African (360 Mg ha^{-1}) and Asian (335 Mg ha^{-1}) forests, followed by intact forests in South America (266 Mg ha^{-1}) and Central America (146 Mg ha^{-1}) (Fig. S6). AGB in non-intact forests was much lower in all regions (Africa, 78 Mg ha^{-1}; Asia, 211 Mg ha^{-1}; South America, 149 Mg ha^{-1}; and Central America, 57 Mg ha^{-1}) (Fig. S6).

Validation

The validation exercise showed that the fused map achieved a lower RMSE (a decrease of 5 – 74%) and bias (a decrease of 90 – 153%) than the input maps for all continents (Fig. 5). While the RMSE of the fused map was consistently lower than that of the input maps but still substantial (87 – 98 Mg ha^{-1}) in the largest continents (Africa, South America and Asia), the mean error (bias) of the fused map was almost null in most cases. Moreover, in the three main continents the bias of the input maps tended to vary with biomass, with overestimation at low values and underestimation at high values, while the errors of the fused map were more consistently distributed (Fig. 6). When computing the error statistics for the pan-tropics (Baccini extent) as the average of the regional validation results weighted by the respective area coverage, the mean bias (in absolute terms) for the fused, Saatchi and Baccini maps was 5, 21 and 28 Mg ha^{-1} and the mean RMSE was 89, 104 and 112 Mg ha^{-1}, respectively (Fig. 5). The accuracy of the input maps reported above was computed using the validation dataset (30% of the reference dataset) to be consistent with the accuracy of the fused map. The accuracy of the input maps was also computed using all reference data and the results (Table S3) were similar to those based on the validation dataset.

Uncertainty map

The uncertainty of the model predictions indicated that the standard deviation of the error of the fused map for each stratum was in the range 11 - 108 Mg ha^{-1}, with largest uncertainties in areas with largest AGB estimates (Congo basin, Eastern Amazon basin and Borneo). When computed in relative terms (as a percentage of the AGB estimate), the model uncertainties presented opposite patterns, with uncertainties larger than the estimates (> 100%) in the low AGB areas (< 20 Mg ha^{-1} on average) of Africa, South America and Central America, while high AGB forests (> 210 Mg ha^{-1} on average) had uncertainties lower than 25% (Fig. 7). The uncertainty measure derived from $\boldsymbol{C}(s)$ was computed only when two or more input maps were available. Hence, it could not be calculated for Australia because the model for this continent was based on only one input map (Saatchi map).

Discussion

Biomass patterns and stocks emerging from the reference data

The AGB map produced with the fusion approach is largely driven by the reference dataset and essentially the method is aimed at spatializing the AGB patterns indicated by the reference data using the support of the input maps. For this reason, great care was taken in the pre-processing of the reference data, which included a two-step quality screening based on metadata analysis and visual interpretation, and their consolidation after stratification. As a result, the reference dataset provides an unprecedented compilation of AGB estimates at 1-km resolution for the tropical region, covering a wide range of vegetation types, biomass ranges and ecological regions across the tropics. It includes the most comprehensive and accurate tropical field plot networks and high-quality maps calibrated with airborne LiDAR, which provide more accurate estimates compared to those obtained from other sensors (Zolkos et al., 2013). The main trends present in the fused map emerged from the combination of different and independent reference datasets and are in agreement with the estimates derived from long-term research plot networks (Malhi et al., 2006; Phillips et al., 2009; Lewis et al., 2009; Slik et al., 2010, 2013; Lewis et al., 2013) and high-resolution maps (Asner et al., 2012a, 2012b, 2013, 2014a). Specifically, the AGB patterns in South America represent spatial trends described by research plot networks in the dense intact and non-intact forests in the Amazon basin, forest inventory plots collected in the dense forests of Guyana and samples extracted from AGB maps for Colombia and Peru representing a wide range of vegetation types, from arid grasslands to humid forests. Similarly, AGB patterns depicted in Africa were derived from a combination of various research plots in dense undisturbed forest (Gabon, Cameroon, Democratic Republic of Congo, Ghana, Liberia), inventory plots in forest concessions (Democratic Republic of Congo), AGB maps in woodland and savannah ecosystems (Uganda, Mozambique) and research plots and maps in montane forests (Ethiopia,

545 Madagascar). Most vegetation types in Central America, Asia and Australia were also well-
546 represented by the extensive forest inventory plots (Indonesia, Vietnam and Laos) and high-
547 resolution maps (Mexico, Panama, Australia).
548
549 In spite of the extensive coverage, the current database is far from being representative of the
550 AGB variability across the tropics. As a consequence, the model estimates are expected to be
551 less accurate in contexts not adequately represented. In the case of the fusion approach, this
552 corresponds to the areas where the input maps present error patterns different than those
553 identified in areas with reference data: in such areas the model parameters used to correct the
554 input maps (bias and weight) may not adequately reflect the errors of the input maps and
555 hence cannot optimally correct them. In particular, deciduous vegetation and heavily
556 disturbed forest of Africa and South America, and large parts of Asia were lacking quality
557 reference data. Moreover, even though plot data were spatially distributed over the central
558 Amazon and the Congo basin, large extents of these two main blocks of tropical forest have
559 never been measured (cf. maps in Lewis et al., 2013; Mitchard et al., 2014). Considering the
560 evidence of significant local differences in forest structure and AGB density within the same
561 forest ecosystems (Kearsley et al., 2013), additional data are needed to strengthen the
562 confidence of the fused map as well as that of any other AGB map covering the tropical
563 region. Moreover, a dedicated gap analysis to assess the main regions lacking AGB reference
564 data and identify priority areas for new field sampling and LiDAR campaigns would be very
565 valuable for future improved biomass mapping.
566
567 Regarding the AGB stocks, a previous study showed that despite their often very strong local
568 differences, the two input maps tended to provide similar estimates of total stocks at national
569 and biome scales and presented an overall net difference of 10% for the pan-tropics (Mitchard

et al., 2013). However, such convergence is mostly due to compensation of contrasting estimates when averaging over large areas. The larger differences with the estimates of the present study (9% and 18%) suggest an overestimation of the total stocks by the input maps. This is in agreement with the results of two previous studies that, on the basis of reference maps obtained by field-calibrated airborne LiDAR data, identified an overestimation of 23% - 42% of total stocks in the Saatchi and Baccini maps in the Colombian Amazon (Mitchard et al., 2013) and a mean overestimation of about 100 Mg ha^{-1} for the Baccini map in the Colombian and Peruvian Amazon (Baccini and Asner, 2013).

In general, the AGB density values of the fused map were calibrated and therefore in agreement with the existing estimates obtained from plot networks and high-resolution maps. The comparison of mean AGB values in intact and non-intact forests stratified by ecozone provided further information on the differences between the maps. The mean AGB values of the fused map in non-intact forests were mostly lower than those of the input maps, suggesting that in disturbed forests the AGB estimates derived from stand height parameters retrieved by spaceborne LiDAR (as in the input maps) tend to be higher compared to those based on tree parameters or very high-resolution airborne LiDAR measurements (as in the fused map and reference data). This difference occurred especially in Africa, Asia and Central America while it was less evident in South America and Australia. By contrast, the differences among the maps for intact forests varied by continent, with the fused map having, on average, higher mean AGB values in Africa, Asia and Australia, lower values in Central America, and variable trends within South America, reflecting the different allometric relationships used by the various datasets in different continents.

As mentioned above, a larger amount of reference data, ideally acquired based on a clear statistical sampling design instead of one that is opportunistic, will be required to confirm such conclusions. While dense sampling of tropical forests using field observations is often impractical, new approaches combining sufficient ground observations of individual trees at calibration plots with airborne LiDAR measurements for larger sampling transects would allow a major increase in the quantity of calibration data. In combination with wall-to-wall medium resolution satellite data (e.g., Landsat) these may be capable of achieving high accuracy over large areas (10% - 20% uncertainty at 1-ha scale) while being cost-effective (e.g., Asner et al., 2013, 2014b). In addition, new technologies, such as Terrestrial Laser Scanning (TLS), allows for better estimates at ground level (Calders et al., 2015; Gonzalez de Tanago et al., 2015), considerably reducing the uncertainties of field estimates based on generalized allometric equations and avoiding destructive sampling. Nevertheless, since floristic composition influences AGB at multiple scales (e.g., the strong pan-Amazon gradient in wood density shown by ter Steege et al., 2006) such techniques benefit from extensive and precise measurements of tree identity in order to determine wood density patterns and to account for variations in hollow stems and rottenness (Nogueira et al., 2006). Moreover, we note that the reference data do not include lianas, which may constitute a substantial amount of woody stems, and their inclusion would allow to obtain more correct estimates of total AGB of vegetation (Phillips et al., 2002; Schnitzer & Bongers, 2011; Durán & Gianoli, 2013).

Additional error sources

Apart from the uncertainty of the fusion model described above (see 'Uncertainty'), three other sources of error were identified and assessed in the present approach: i) errors in the reference dataset; ii) errors due to temporal mismatch between the reference data and the input maps; iii) errors in the stratification map.

619

620 **Errors in the reference dataset**

621 The reference dataset is not error-free but it inherits the errors present in the field data and
622 local maps. In addition, additional uncertainties are introduced during the pre-processing of
623 the data by resampling the maps and upscaling the plot data to 1-km resolution. In particular,
624 while the geolocation error of the original datasets was considered relatively small (< 50 m)
625 since plot coordinates were collected using GPS measurements and the AGB maps were
626 based on satellite data with accurate geolocation (i.e., Landsat, ALOS, MODIS), larger errors
627 (up to 500 m, half a pixel) could have been introduced with the resampling of the 1-km input
628 maps. All these error sources were minimized by selecting only the datasets that fulfilled
629 certain quality criteria and by further screening them through visual analysis of high-
630 resolution images available on the Google Earth platform, discarding the data not
631 representative of the respective map pixels. In case of reference data that clearly did not
632 match with the high-resolution images and/or with the input maps (e.g., reporting no AGB in
633 dense forest areas or high AGB on bare land), the data were considered as an error in the
634 reference dataset, a geolocation error in the plots or maps, or it was assumed that a land
635 change process occurred between the plot measurement and the image acquisition time (see
636 next paragraph).

637

638 **Errors due to temporal mismatch**

639 The temporal difference of input and reference data introduced some uncertainty in the fusion
640 model. The input maps refer to the years 2000 – 2001 (Saatchi) and 2007 – 2008 (Baccini)
641 while the reference data mostly spanned the period 2000 – 2013. Therefore, the differences
642 between the input maps and the reference data may also be due to a temporal mismatch of the
643 datasets. However, changes due to deforestation were most likely excluded during the visual

644 selection of the reference data, when high-resolution images showed clear land changes (e.g.,
645 bare land or agriculture) in areas where the input maps provided AGB estimates relative to
646 forest areas (or *vice-versa*, depending on the timing of acquisition of the datasets). However,
647 changes due to forest regrowth and degradation events that did not affect the forest canopy
648 could not be considered with the visual analysis and may have affected the mismatch
649 observed between the reference data and the input maps (< 58 – 80 Mg ha^{-1} for 50% of the
650 cases of the Saatchi and Baccini maps, respectively). Part of the mismatch was in the range of
651 AGB changes that can be attributes to regrowth (1 – 13 Mg ha^{-1} $year^{-1}$) (IPCC, 2003) or low-
652 intensity degradation (14 – 100 Mg ha^{-1}, or 3 – 15% of total stock) (Asner et al., 2010;
653 Pearson et al., 2014). On the other hand, considering the limited area affected by degradation
654 (about 20% in the humid tropics) (Asner et al., 2009), the temporal mismatch could be
655 responsible only for a correspondent part of the differences observed between the reference
656 data and the input maps. Small additional offsets may also be caused by the documented
657 secular changes in AGB density within intact tropical forests, which has been increasing by
658 0.2 – 0.5% per year (Phillips et al., 1998, Chave et al., 2008, Phillips and Lewis, 2014). It
659 should also be noted that the reference data were used to optimally integrate the input maps,
660 and in the case of a temporal difference the fused map was 'actualized' to the state of the
661 vegetation when the reference data were acquired. The reference data were acquired between
662 2000 and 2013, and their mean acquisition year weighted by their contribution to the fusion
663 model (by continent) corresponds to the period 2007 – 2010 (2007 in Africa, 2008 in Central
664 America, 2009 in South America and 2010 in Asia). Therefore the complete fused map cannot
665 be attributed to a specific year and more generally it represents the first decade of the 2000s.
666
667 **Errors in the stratification map**

668 The errors in the stratification map (i.e., related to the prediction of the errors of the input
669 maps) were still substantial in some areas and affected the fused map in two ways. First, the
670 reference data that were erroneously attributed to a certain stratum introduced 'noise' in the
671 estimation of the model parameters (bias and weight), but the impact of these 'outliers' was
672 largely reduced by the use of a robust covariance estimator. Second, erroneous predictions of
673 the strata caused the use of incorrect model parameters in the combination of the input maps.
674 The latter is considered to be the main source of error of the fused map and indicates that the
675 method can achieve improved results if the errors of the input maps can be predicted more
676 accurately. However, additional analysis showed that, on average, fused maps based on
677 alternative stratification approaches achieved lower accuracy than the map based on an error
678 stratification approach (Fig. S5). Therefore, this approach was preferred over a stratification
679 based on an individual biophysical variable (e.g., tree cover, tree height, land cover or
680 ecozone).
681
682 ***Application of the method at national scale***
683 The fusion method presented in this study allows for the optimal integration of any number of
684 input maps to match the patterns indicated by the reference data. However, the accuracy of the
685 fused map depends on the availability of reference data representative of the error patterns of
686 the input maps. While the current reference database does not represent adequately all error
687 strata for the tropical region, and the model estimates are expected to have lower confidence
688 in under-represented areas, the proposed method may be applied locally and provide
689 improved AGB estimates where additional reference data are available. For example, the
690 fusion method may be applied at national level using existing forest inventory data, research
691 plots and local maps that cover only part of the country to calibrate global or regional maps,
692 which provide national coverage but may not be tailored to the country context. Such country-

693 calibrated AGB maps may be used to support natural resource management and national
694 reporting under the REDD+ mechanism, especially for countries that have limited capacities
695 to map AGB from remote sensing data (Romijn et al., 2012). Considering the increasing
696 number of global or regional AGB datasets based on different data and methodologies
697 expected in the coming years, and that likely there will not be a single 'best map' but rather
698 the accuracy of each will vary spatially, the fusion approach may allow to optimally combine
699 and adjust available datasets to local AGB patterns identified by reference data.
700
701
702
703
704
705
706
707
708
709
710
711
712
713
714
715
716
717

Acknowledgments

This study was supported by the EU FP7 GEOCARBON (283080) project, by NORAD (grant agreement no. QZA-10/0468) and AusAID (grant agreement no. 46167) within CIFOR's Global Comparative Study on REDD+. This work was further supported by the German Federal Ministry for the Environment, Nature Conservation and Nuclear Safety (BMU) International Climate Initiative (IKI) through the project "From Climate Research to Action under Multilevel Governance: Building Knowledge and Capacity at Landscape Scale". Data were also acquired and/or collated by the Sustainable Landscapes Brazil project supported by the Brazilian Agricultural Research Corporation (EMBRAPA), the US Forest Service and USAID, and the US Department of State, Aberystwyth University, the University of New South Wales (UNSW), and the Queensland Department of Science, Information Technology and Innovation (DSITI). GP Asner and the Carnegie Airborne Observatory were supported by the Avatar Alliance Foundation, John D. and Catherine T. MacArthur Foundation, and NSF grant 1146206. OP, SLL and LQ acknowledge the support of the European Research Council (T-FORCES), TS, LQ and SLL were supported by CIFOR/USAID; SLL was also supported by a Philip Leverhulme Prize. LQ thanks the Forestry Department Sarawak, Sabah Biodiversity Council, State Ministry of Research and Technology (RISTEK) Indonesia for permissions to carry out the 2013-2014 recensus of long-term forest plots in Borneo (a subset of which included as Cluster AS16), and Lip Khoon Kho, Sylvester Tan, Haruni Krisnawati and Edi Mirmanto for field assistance and accessing plot data.

References

Achard F, Beuchle R, Mayaux P et al. (2014) Determination of tropical deforestation rates and related carbon losses from 1990 to 2010. *Global Change Biology*, **20**, 2540–2554.

Asner GP, Clark JK, Mascaro J et al. (2012a) High-resolution mapping of forest carbon stocks in the Colombian Amazon. *Biogeosciences*, **9**, 2683–2696.

Asner GP, Clark JK, Mascaro J et al. (2012b) Human and environmental controls over aboveground carbon storage in Madagascar. *Carbon Balance and Management*, **7**, 2.

Asner GP, Mascaro J, Anderson C et al. (2013) High-fidelity national carbon mapping for resource management and REDD+. *Carbon balance and management*, **8**, 7.

Asner GP, Knapp DE, Martin RE et al. (2014a) Targeted carbon conservation at national scales with high-resolution monitoring. *Proceedings of the National Academy of Sciences*, **111**, E5016–E5022.

Asner GP, Mascaro J (2014b) Mapping tropical forest carbon: Calibrating plot estimates to a simple LiDAR metric. *Remote Sensing of Environment*, **140**, 614–624.

Avitabile V, Herold M, Henry M, Schmullius C (2011) Mapping biomass with remote sensing: a comparison of methods for the case study of Uganda. *Carbon Balance and Management*, **6**, 7.

Avitabile V, Baccini A, Friedl MA, Schmullius C (2012) Capabilities and limitations of Landsat and land cover data for aboveground woody biomass estimation of Uganda. *Remote Sensing of Environment*, **117**, 366–380.

Baccini A, Goetz SJ, Walker WS et al. (2012) Estimated carbon dioxide emissions from tropical deforestation improved by carbon-density maps. *Nature Climate Change*, **2**, 182–185.

Baccini A, Asner GP (2013) Improving pantropical forest carbon maps with airborne LiDAR sampling. *Carbon Management*, **4**, 591–600.

768 Bartholomé E, Belward a. S (2005) GLC2000: a new approach to global land cover mapping
769 from Earth observation data. *International Journal of Remote Sensing*, **26**, 1959–1977.
770 Bates JM, Granger CWJ (1969) The Combination of Forecasts. *Journal of the Operational*
771 *Research Society*, **20**, 451–468.
772 Birdsey R, Angeles-Perez G, Kurz W a et al. (2013) Approaches to monitoring changes in
773 carbon stocks for REDD+. *Carbon Management*, **4**, 519–537.
774 Breiman L (2001) Random forests. *Machine Learning*, **45**, 5−23.
775 Calders K, Newnham G, Burt A et al. (2015) Nondestructive estimates of above-ground
776 biomass using terrestrial laser scanning. *Methods in Ecology and Evolution*, **6**, 198–208.
777 Cartus O, Kellndorfer J, Walker W, Franco C, Bishop J, Santos L, Michel-Fuentes JM (2014)
778 A National, Detailed Map of Forest Aboveground Carbon Stocks in Mexico. *Remote*
779 *Sensing*, **6**, 5559–5588.
780 Chave J, Olivier J, Bongers F et al. (2008) Above-ground biomass and productivity in a rain
781 forest of eastern South America. *Journal of Tropical Ecology*, **24**, 355–366.
782 DiMiceli CM, Carroll ML, Sohlberg RA et al. (2011) Annual Global Automated MODIS
783 Vegetation Continuous Fields (MOD44B) at 250 m Spatial Resolution for Data Years
784 Beginning Day 65, 2000 - 2010, Collection 5 Percent Tree Cover, University of
785 Maryland, College Park, MD, USA
786 ESA (2014a) Global land cover map for the epoch 2005. http://www.esa-landcover-cci.org/
787 ESA (2014b) Global Water Bodies. http://www.esa-landcover-cci.org/
788 FAO (2000) Global ecological zoning for the global forest resources assessment 2000. FAO
789 FRA Working Paper Rome, Italy; 2001
790 Feldpausch TR, Banin L, Phillips OL et al. (2011) Height-diameter allometry of tropical
791 forest trees. *Biogeosciences*, **8**, 1081–1106.

792 Feldpausch TR, Lloyd J, Lewis SL et al. (2012) Tree height integrated into pantropical forest
793 biomass estimates. *Biogeosciences*, **9**, 3381–3403.
794 Ge Y, Avitabile V, Heuvelink GBM, Wang J, Herold M (2014) Fusion of pan-tropical
795 biomass maps using weighted averaging and regional calibration data. *International*
796 *Journal of Applied Earth Observation and Geoinformation*, **31**, 13–24.
797 Goetz S, Dubayah R (2011) Advances in remote sensing technology and implications for
798 measuring and monitoring forest carbon stocks and change. *Carbon Management*, **2**,
799 231–244.
800 Gonzalez de Tanago J, Bartholomeus H, Joseph S et al. (2015) Terrestrial LiDAR and 3D tree
801 Quantitative Structure Model for quantification of aboveground biomass loss from
802 selective logging in a tropical rainforest of Peru. In: *Proceedings of Silvilaser 2015*
803 *Conference. La Grande Motte, France. 28-30 September 2015*.
804 Grace J, Mitchard E, Gloor E (2014) Perturbations in the carbon budget of the tropics. *Global*
805 *Change Biology*.
806 Harris NL, Brown S, Hagen SC et al. (2012) Baseline Map of Carbon Emissions from
807 Deforestation in Tropical Regions. *Science*, **336**, 1573–1576.
808 Hill TC, Williams M, Bloom A, Mitchard ET, Ryan CM (2013) Are Inventory Based and
809 Remotely Sensed Above-Ground Biomass Estimates Consistent? *PLoS ONE*, **8**, 1–8.
810 Houghton RA, House JI, Pongratz J et al. (2012) Carbon emissions from land use and land-
811 cover change. *Biogeosciences*, **9**, 5125–5142.
812 Jiahui W, Zamar R, Marazzi A, et al. (2014) robust: Robust Library. R package version 0.4-
813 16. http://CRAN.R-project.org/package=robust.
814 Kearsley E, de Haulleville T, Hufkens K et al. (2013) Conventional tree height-diameter
815 relationships significantly overestimate aboveground carbon stocks in the Central Congo
816 Basin. *Nature communications*, **4**, 2269.

817 IPCC (2003) Good practice guidance for land use, land-use change and forestry. IPCC
818 National Greenhouse Gas Inventories Programme, Technical Support Unit. Hayama,
819 Japan: Institute for Global Environmental Strategies.
820 IPCC (2006) 2006 IPCC Guidelines for National Greenhouse Gas Inventories, Prepared by
821 the National Greenhouse Gas Inventories Programme, Eggleston HS, Buendia L, Miwa
822 K, Ngara T and Tanabe K (eds). Published: IGES, Japan.
823 Langner A, Achard F, Grassi G (2014) Can recent pan-tropical biomass maps be used to
824 derive alternative Tier 1 values for reporting REDD+ activities under UNFCCC?
825 *Environmental Research Letters*, **9**, 124008.
826 Lewis SL, Lopez-Gonzalez G, Sonké B et al. (2009) Increasing carbon storage in intact
827 African tropical forests. *Nature*, **457**, 1003–1006.
828 Lewis SL, Sonké B, Sunderland T et al. (2013) Above-ground biomass and structure of 260
829 African tropical forests. *Philosophical transactions of the Royal Society of London.*
830 *Series B, Biological sciences*, **368**, 20120295.
831 Malhi Y, Wood D, Baker TR et al. (2006) The regional variation of aboveground live biomass
832 in old-growth Amazonian forests. *Global Change Biology*, **12**, 1107–1138.
833 Mitchard ET, Saatchi SS, Baccini A, Asner GP, Goetz SJ, Harris NL, Brown S (2013)
834 Uncertainty in the spatial distribution of tropical forest biomass: a comparison of pan-
835 tropical maps. *Carbon balance and management*, **8**, 10.
836 Mitchard ET, Feldpausch TR, Brienen RJW et al. (2014) Markedly divergent estimates of
837 Amazon forest carbon density from ground plots and satellites. *Global Ecology and*
838 *Biogeography*, **23**, 935–946.
839 Nogueira MA, Diaz G, Andrioli W, Falconi FA, Stangarlin JR (2006) Secondary metabolites
840 from Diplodia maydis and Sclerotium rolfsii with antibiotic activity. *Brazilian Journal of*
841 *Microbiology*, **37**, 14–16.

842 Pan Y, Birdsey RA, Fang J et al. (2011) A large and persistent carbon sink in the world's
843 forests. *Science*, **333**, 988–993.
844 Pearson TRH, Brown S, Casarim FM (2014) Carbon emissions from tropical forest
845 degradation caused by logging. *Environmental Research Letters*, **034017**, 11.
846 Phillips O L, Malhi Y, Higuchi N et al. (1998) Changes in the carbon balance of Tropical
847 Forests: Evidence from long-term plots. *Science*, **282**, 439–442.
848 Phillips OL, Aragão LEOC, Lewis SL et al. (2009) Drought sensitivity of the Amazon
849 Rainforest. *Science*, **323**, 1344–1347.
850 Phillips OL, Lewis SL (2014) Evaluating the tropical forest carbon sink. *Global Change*
851 *Biology*, **20**, 2039–2041.
852 Potapov P, Yaroshenko A, Turubanova S et al. (2008) Mapping the world's intact forest
853 landscapes by remote sensing. *Ecology and Society*, **13**.
854 Romijn E, Herold M, Kooistra L, Murdiyarso D, Verchot L (2012) Assessing capacities of
855 non-Annex I countries for national forest monitoring in the context of REDD+.
856 *Environmental Science and Policy*, **19-20**, 33–48.
857 Saatchi SS, Harris NL, Brown S et al. (2011) Benchmark map of forest carbon stocks in
858 tropical regions across three continents. *Proceedings of the National Academy of*
859 *Sciences*, 108, 9899–9904.
860 Saatchi SS, Mascaro J, Xu L et al. (2014) Seeing the forest beyond the trees. *Global Ecology*
861 *& Biogeography*, **23**, 935 – 946.
862 Searle SR (1971) *Linear Models*, Vol. XXI. WILEY-VCH Verlag, York-London-Sydney-
863 Toronto, 532 pp.
864 Simard M, Pinto N, Fisher JB, Baccini A (2011) Mapping forest canopy height globally with
865 spaceborne lidar. Journal of Geophysical Research: Biogeosciences, 116, 1–12.

866 Slik JWF, Aiba SI, Brearley FQ et al. (2010) Environmental correlates of tree biomass, basal
867 area, wood specific gravity and stem density gradients in Borneo's tropical forests.
868 *Global Ecology and Biogeography*, **19**, 50–60.
869 Slik JWF, Paoli G, Mcguire K et al. (2013) Large trees drive forest aboveground biomass
870 variation in moist lowland forests across the tropics. *Global Ecology and Biogeography*,
871 **22**, 1261–1271.
872 Ter Steege H, Pitman NC a, Phillips OL et al. (2006) Continental-scale patterns of canopy
873 tree composition and function across Amazonia. *Nature*, **443**, 444–447.
874 Willcock S, Phillips OL, Platts PJ et al. (2012) Towards Regional, Error-Bounded Landscape
875 Carbon Storage Estimates for Data-Deficient Areas of the World. *PLoS ONE*, **7**, 1–10.
876 Wright JS (2013) The carbon sink in intact tropical forests. *Global Change Biology*, **19**, 337–
877 339.
878 Ziegler AD, Phelps J, Yuen JQ et al. (2012) Carbon outcomes of major land-cover transitions
879 in SE Asia: Great uncertainties and REDD+ policy implications. *Global Change*
880 *Biology*, **18**, 3087–3099.
881 Zolkos SG, Goetz SJ, Dubayah R (2013) A meta-analysis of terrestrial aboveground biomass
882 estimation using lidar remote sensing. *Remote Sensing of Environment*, **128**, 289–298.
883
884
885
886
887
888
889
890

Supporting Information

Appendix S1. Supplementary methods and results

912 # Tables

913 **Table 1: Number of reference data (plots and 1-km pixels) selected after the screening, upscaling and**
914 **consolidating procedures, per continent. The reference data selected for each individual dataset are**
915 **reported in Table S1. The field plots underpinning the reference AGB maps are not included.**

Continent	Available	Selected		Consolidated
	Plots	*Plots*	*Pixels*	*Pixels*
Africa	2,281	1,976	953	953
S. America	648	474	449	449
C. America	-	-	5,260	7,675
Asia	3,698	1,833	353	400
Australia	-	-	5,000	5,000
Total	**6,627**	**4,283**	**12,015**	**14,477**

916
917
918
919
920
921
922
923
924
925
926
927

928 ## Figure captions

929 **Figure 1: Flowchart illustrating the methods for generating the fused biomass map and associated**
930 **uncertainty**

931 **Figure 2: AGB reference dataset for the tropics and spatial coverage of the two input maps**

932 **Figure 3: Fused map, representing the distribution of live woody aboveground biomass (AGB) for all land**
933 **cover types at 1-km resolution for the tropical region.**

934 **Figure 4: Difference maps obtained by subtracting the fused map from the Saatchi map (a) and the**
935 **Baccini map (b).**

936 **Figure 5: RMSE (a) and bias (b) of the fused and input maps per continent obtained using independent**
937 **reference data not used for model development. The error bars indicate one standard deviation of the 100**
938 **simulations. Numbers reported in brackets indicate the number of reference observations used for each**
939 **continent. The results for the pan-tropics exclude Australia, which is not covered by the Baccini map.**

940 **Figure 6: scatterplots of the validation reference data (x-axis) and predictions (y-axis) of the input maps**
941 **(left plots) and fused map (right plots) by continent.**

942 **Figure 7: Uncertainty of the fused map, in absolute values (a) and relative to the AGB estimates (b),**
943 **representing one standard deviation of the error of the fused map.**

944

945

946

947

948

949

950

951

952

953

954

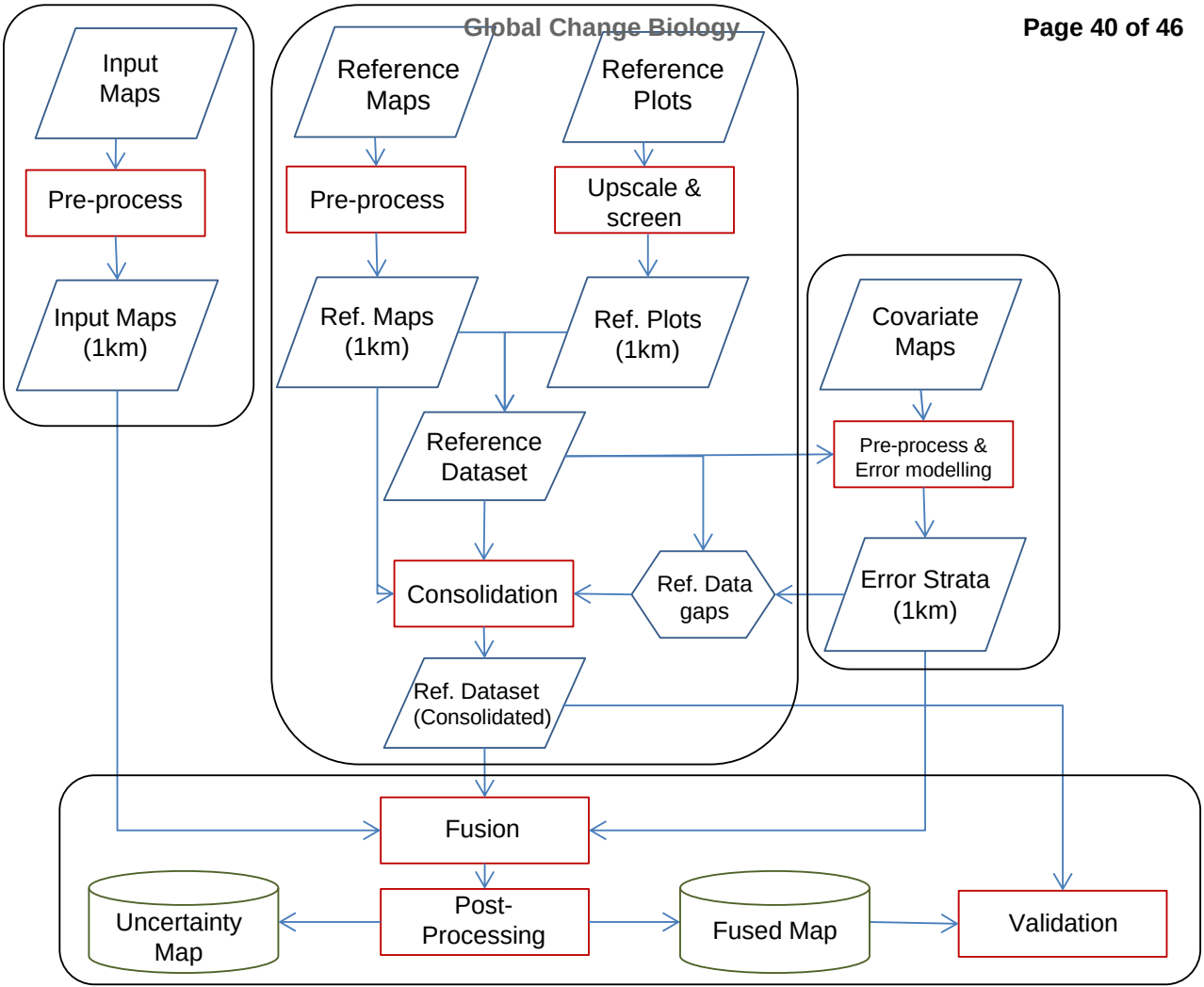
Input Maps
Pre-process
Input Maps (1km)
Reference Maps
Reference Plots
Pre-process
Upscale & screen
Ref. Maps (1km)
Ref. Plots (1km)
Reference Dataset
Consolidation
Ref. Data gaps
Ref. Dataset (Consolidated)
Covariate Maps
Pre-process & Error modelling
Error Strata (1km)
Fusion
Uncertainty Map
Post-Processing
Fused Map
Validation

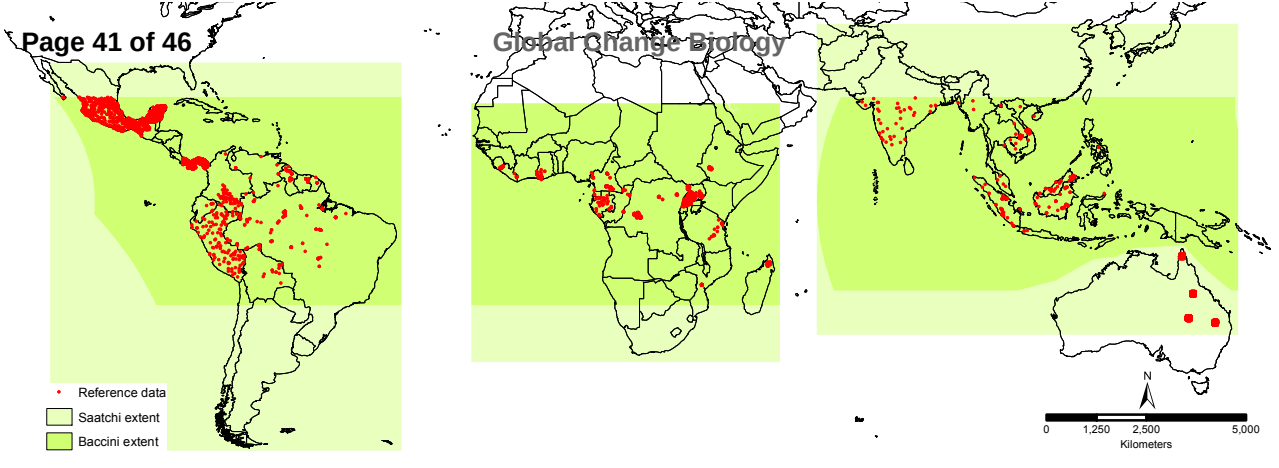
Reference data
Saatchi extent
Baccini extent
N
0
1,250
2,500
5,000
Kilometers

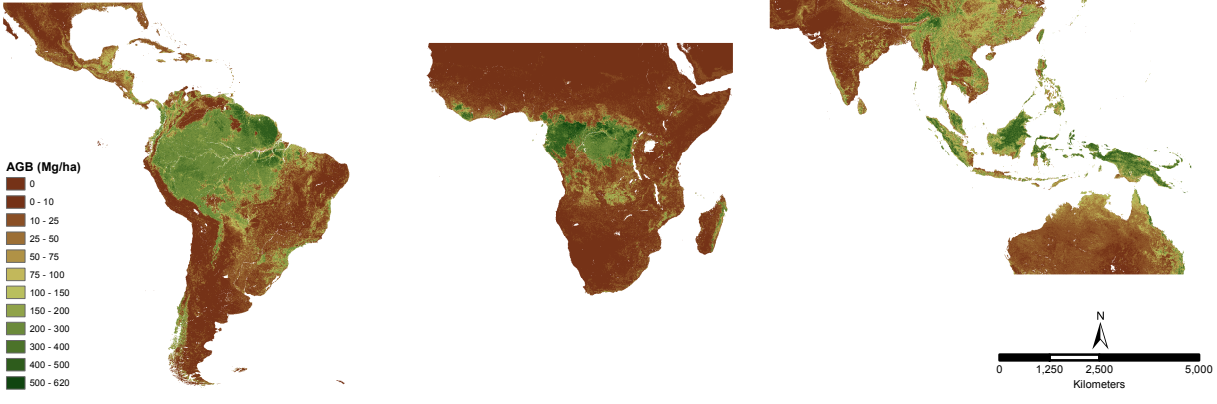
AGB (Mg/ha)
0
0 - 10
10 - 25
25 - 50
50 - 75
75 - 100
100 - 150
150 - 200
200 - 300
300 - 400
400 - 500
500 - 620
N
0
1,250
2,500
5,000
Kilometers

(a)

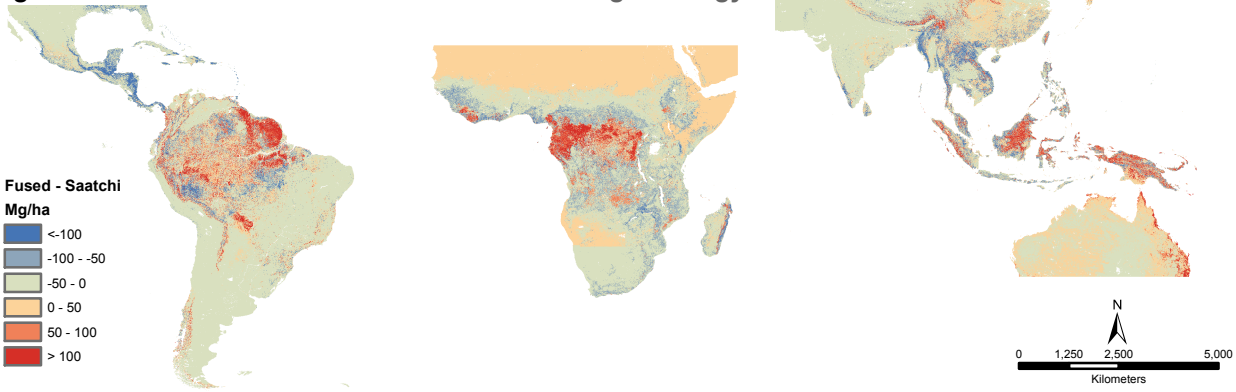
Fused - Saatchi
Mg/ha
<-100
-100 - -50
-50 - 0
0 - 50
50 - 100
> 100
N
0
1,250
2,500
5,000
Kilometers

(b)

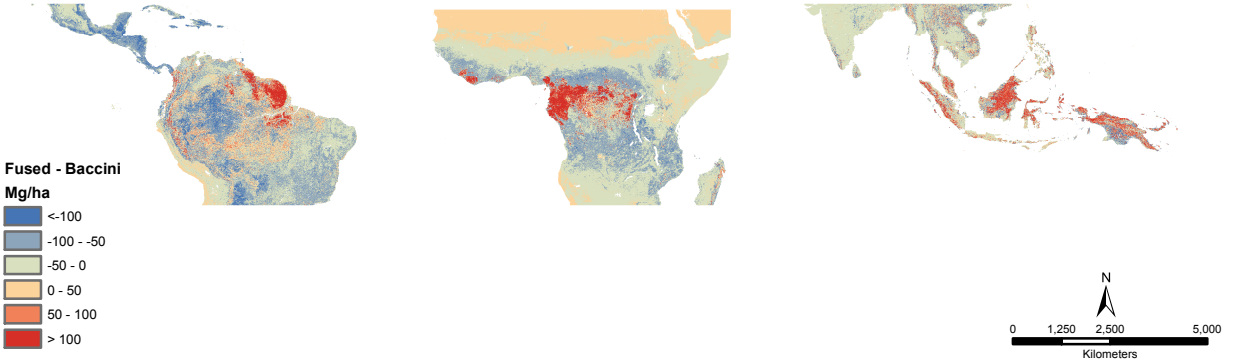
Fused - Baccini
Mg/ha
<-100
-100 - -50
-50 - 0
0 - 50
50 - 100
> 100
N
0
1,250
2,500
5,000
Kilometers

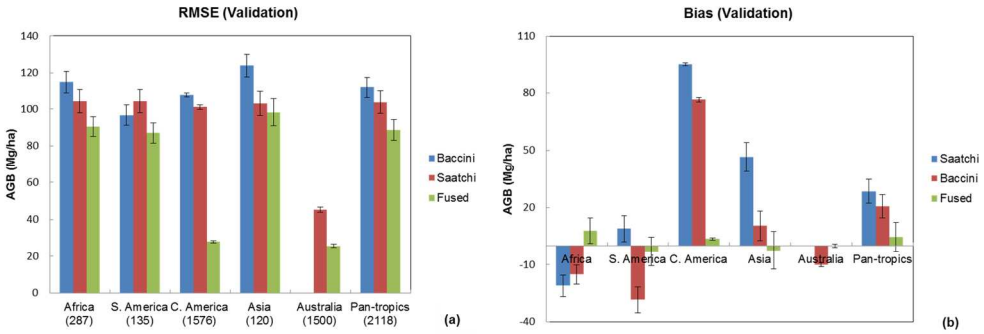

RMSE (a) and bias (b) of the fused and input maps per continent obtained using independent reference data not used for model development. The error bars indicate one standard deviation of the 100 simulations. Numbers reported in brackets indicate the number of reference observations used for each continent. The results for the pan-tropics exclude Australia, which is not covered by the Baccini map.
469x160mm (96 x 96 DPI)

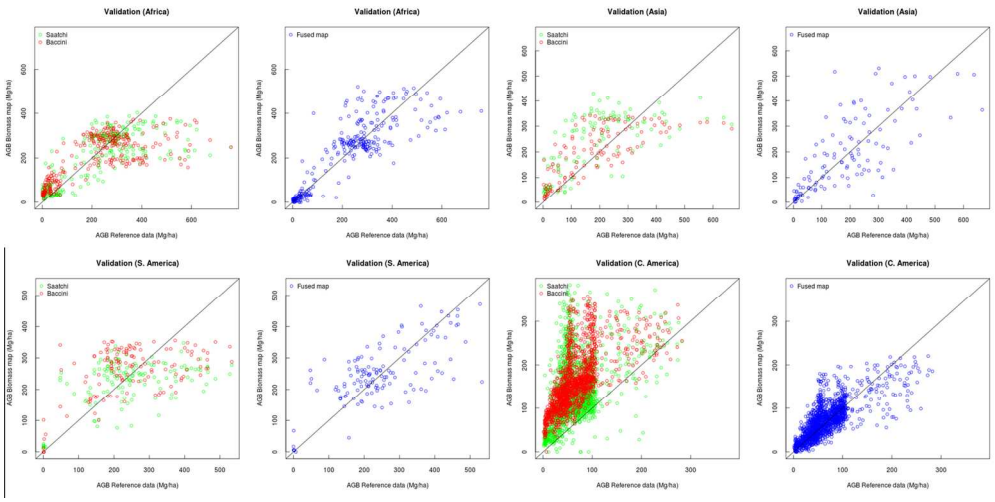

scatterplots of the validation reference data (x-axis) and predictions (y-axis) of the input maps (left plots) and fused map (right plots) by continent.
311x155mm (150 x 150 DPI)

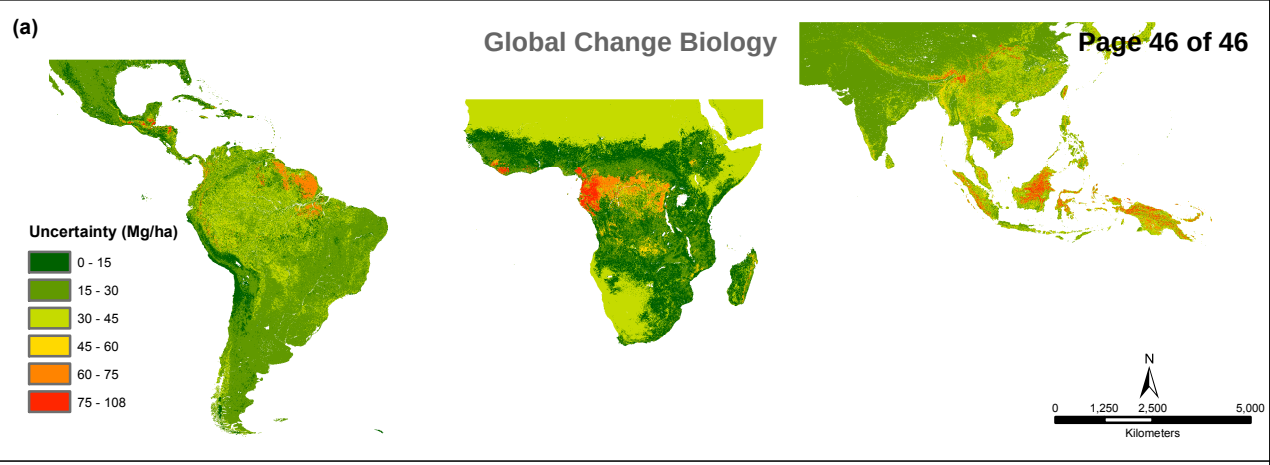
(a)
Uncertainty (Mg/ha)
0 - 15
15 - 30
30 - 45
45 - 60
60 - 75
75 - 108
N
0 1,250 2,500 5,000
Kilometers

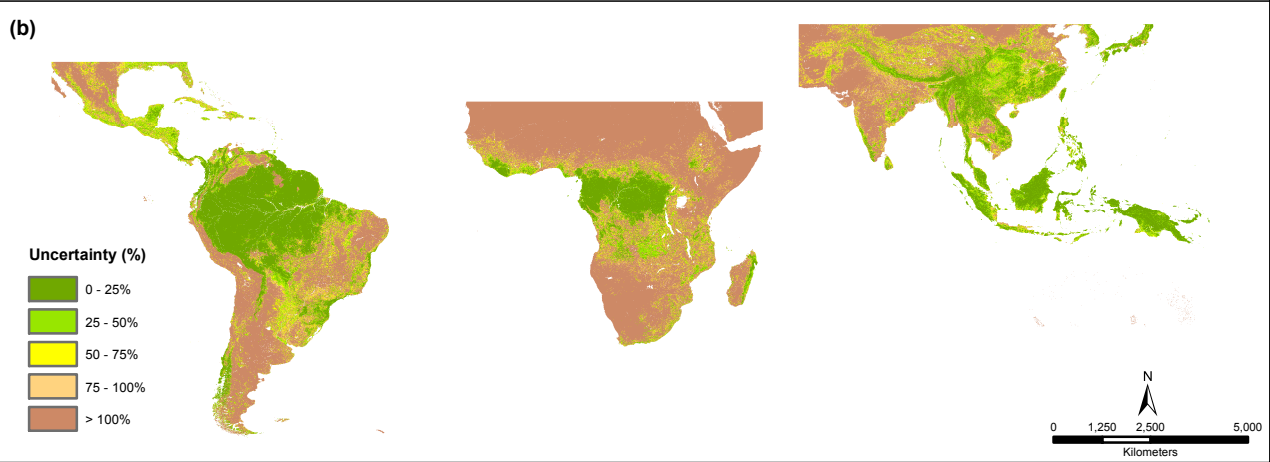
(b)
Uncertainty (%)
0 - 25%
25 - 50%
50 - 75%
75 - 100%
> 100%
N
0 1,250 2,500 5,000
Kilometers